Electronic Supplementary Material (ESI) for Chemical Communications. This journal is ©
The Royal Society of Chemistry 2023

Supporting Information

Deciphering the Roles of Ammonium Doping for Lead-Free $(NH_4)_xCs_{3-x}Cu_2I_5$ Perovskites to Regulate the Photoelectronic Properties

Zeyao Xu[a,b], Linqin Jiang[*b], Hao Xiong[b], Jiansen Wen[c], Ping Li[b], Lingyan Lin[b], Bo Wu[c], Aijun Yang[d], Yu Qiu[*b]

a College of Physics and Information Engineering, Fuzhou University, Fuzhou 350108, China.
b Key Laboratory of Green Perovskites Application of Fujian Provincial Universities, Fujian Jiangxia University, Fuzhou 350108, China, E-mail: linqinjiang@fjjxu.edu.cn, yuqiu@fjjxu.edu.cn.
c Multiscale Computational Materials Facility, Key Laboratory of Eco-Materials Advanced Technology, College of Materials Science and Engineering, Fuzhou University, Fuzhou 350108, China
d PV Metrology Institute, Fujian Metrology Institute, Fuzhou 350003, China.

Experimental

Materials

Cesium iodide (CsI, 99.9%), copper(I) iodide (CuI, 99.5%), ammonium iodide (NH_4I, 99.9%), dimethylsulfoxide (DMSO, 99.8%) and chlorobenzene (C_6H_5Cl, anhydrate,) were all purchased from Aladdin Industrial Corporation.

Synthesis of $(NH_4)_xCs_{3-x}Cu_2I_5$ ($0 \leq x \leq 3$) powders

Under the dry atmospheric conditions, NH_4I, CsI, and CuI were mixed to a 50 ml agate ball mill jar with the weight ratio of x:(3-x):2. The agate grinding balls are composed of 30 pieces of 5 mm grinding balls and 4 pieces of 8 mm grinding balls. The powders were ground using a planetary ball-mill (Changsha MITR Corp., YXQM-4L) at the speed of 1000 rpm for 2h in air. Then the products were removed and stored in a dry box. Typically for the preparation of $(NH_4)_{0.9}Cs_{2.1}Cu_2I_5$ powder, NH_4I (130 mg, 0.9 mmol), CsI (546 mg, 2.1 mmol), and CuI (571 mg, 3 mmol) were mixed evenly and ball-milled. Under the same conditions, $(NH_4)_xCs_{3-x}Cu_2I_5$($0 \leq x \leq 3$) powders with various NH_4I ratios were fabricated.

Fabrication of the perovskite films

The precursor solution was prepared by adding 0.5 mmol of perovskite powder to 1 ml of mixed solution (DMF: DMSO=4:1) at 50°C for 1 h. In a glove box, the filtered solution was spin-coated on the FTO conductive glass substrate with a low-speed spinning (1000 rpm, 15 s) and a high-speed spinning (3000 rpm, 30 s). During the spin-coating process, 100 ul of chlorobenzene was dropwised for the remaining 10 s to form the film. The resulting film was annealed at 100°C for 1h.

Fabrication of the UV-pumped pc-LEDs

Taking $Cs_3Cu_2I_5$-LED as an example. Firstly, $Cs_3Cu_2I_5$ powder (0.1 g) was placed into a small isotope bottle. Then 0.1 g thermal-curable silicone resin OE-6551 A was added to the bottle with stirring intensely. The hardener OE-6551 B (0.2 g) was also mixed to form blue-emitting phosphor paste. Finally, the paste was integrated with the semiconductor LED chip (310 nm, EPILED Co., Ltd). The $(NH_4)_{0.6}Cs_{2.4}Cu_2I_5$ - LED and $(NH_4)_{0.9}Cs_{2.1}Cu_2I_5$ - LED were achieved in the same processes.

Characterization

The crystallinity characterizations of the samples were analyzed by X-ray diffraction (XRD, Ultima IV). The morphologies of the products were analyzed by scanning electron microscope (SEM, TESCAN MIRA LMS). The optical properties of the perovskites were measured by Ultraviolet-visible (UV-vis) absorption

spectroscopy (Shimadzu UV-3600) and steady-state PL spectra (Edinburgh FLS1000) with an excitation line of 300 nm. The photoluminescence quantum efficiency (PLQY) and time-resolved PL (TRPL) decay curves of the $(NH_4)_xCs_{3-x}Cu_2I_5$ ($0 \leq x \leq 3$) samples were determined with the same fluorescence spectrometer. Fourier Transform Infrared Spectroscopy (FTIR, Nicolet, Avatar-360)) is used to test samples for composition analysis and identification. Thermal analysis of the samples is used to perform by thermogravimetric analysis (TG/TGA, NETZSCH STA449C). The X-ray photoelectron spectroscopy (XPS) and ultraviolet photoelectron spectroscopy (UPS) were collected on a Thermo instrument (Thermo ESCALAB 250XI).

Figures and tables

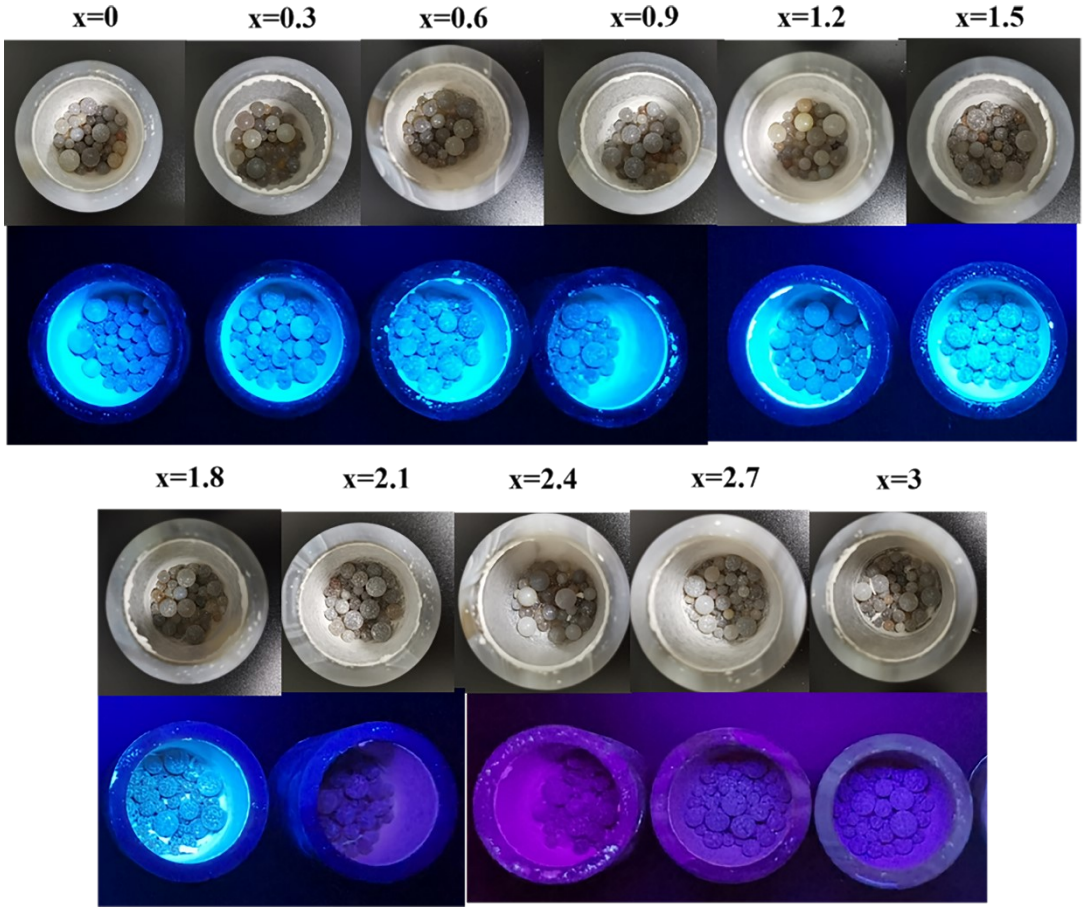

Fig. S1 Images of $(NH_4)_xCs_{3-x}Cu_2I_5$ ($0 \leq x \leq 3$) powders in sunlight (up) and under excitation with a 254nm UV lamp (down).

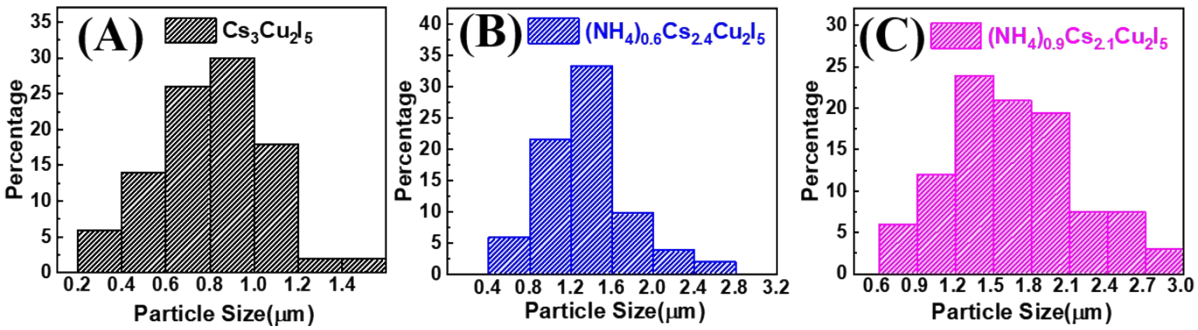

Fig. S2 Size distribution of $(NH_4)_xCs_{3-x}Cu_2I_5$ ($0 \leq x \leq 3$): (A) $Cs_3Cu_2I_5$, (B) $(NH_4)_{0.6}Cs_{2.1}Cu_2I_5$, (C) $(NH_4)_{0.9}Cs_{2.1}Cu_2I_5$.

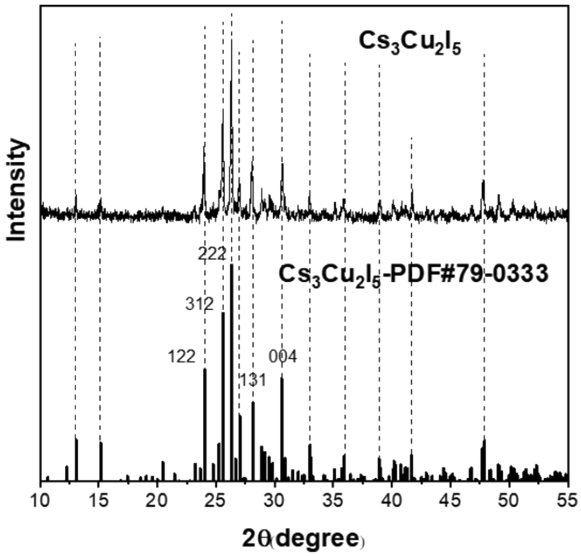

Fig. S3 XRD patterns of $Cs_3Cu_2I_5$ powder prepared by ball milling and standard card of $Cs_3Cu_2I_5$ (PDF#79-0333).

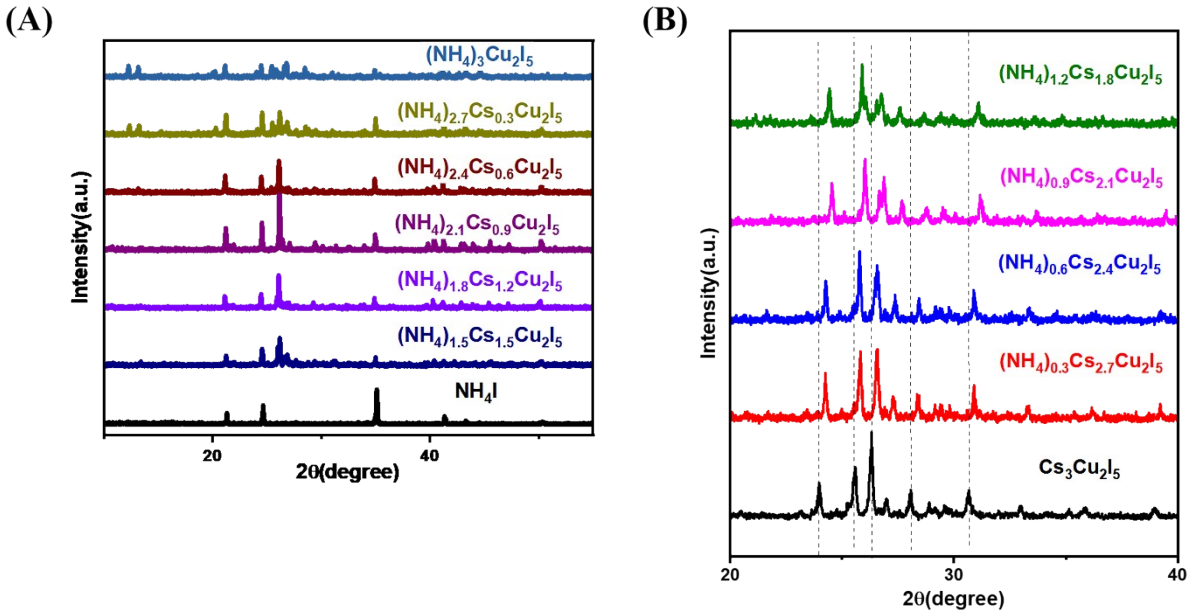

Fig. S4 (a) XRD patterns of $(NH_4)_xCs_{3-x}Cu_2I_5$ ($0 \leq x \leq 3$): x=1.5, x=1.8, x=2.1, x=2.4, x=2.7, x=3 and pure NH_4I. (B) Enlarged XRD patterns at 2θ =20~40° of $(NH_4)_xCs_{3-x}Cu_2I_5$: x=0, x=0.3, x=0.6, x=0.9, x=1.2.

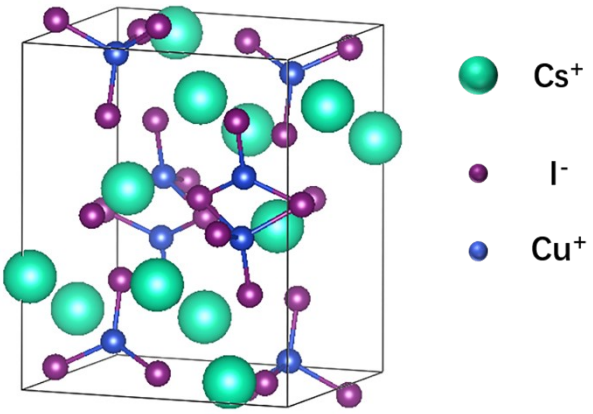

Fig. S5 Crystal structure of $Cs_3Cu_2I_5$.

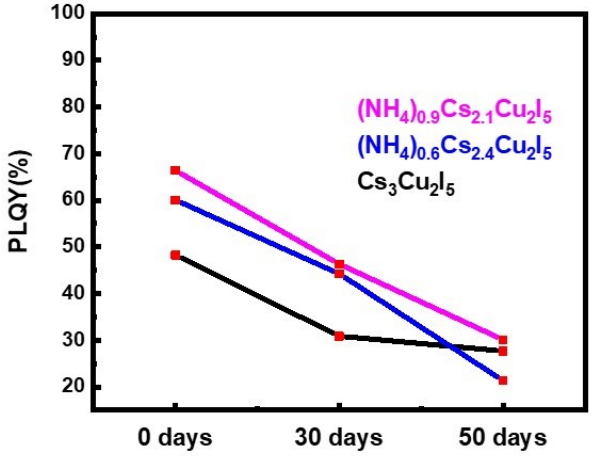

Fig. S6 PLQY of $Cs_3Cu_2I_5$, $(NH_4)_{0.6}Cs_{2.4}Cu_2I_5$ and $(NH_4)_{0.9}Cs_{2.1}Cu_2I_5$ after stored under ambient conditions for 0-50 days.

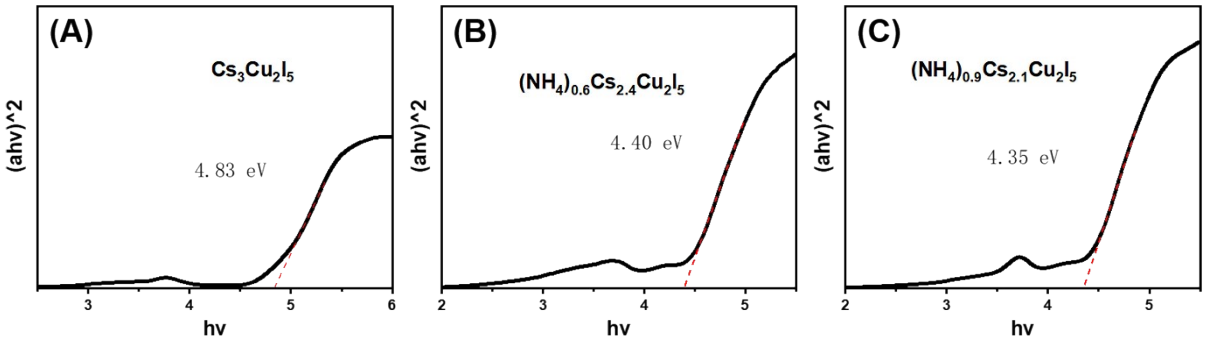

Fig. S7 The Tauc plots of (a) $Cs_3Cu_2I_5$, (b) $(NH_4)_{0.6}Cs_{2.1}Cu_2I_5$, and (c) $(NH_4)_{0.9}Cs_{2.1}Cu_2I_5$.

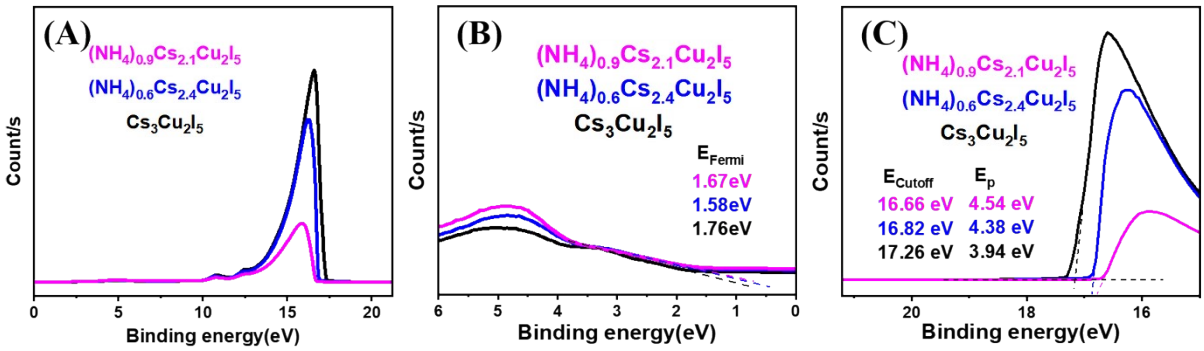

Fig. S8 (a) UPS spectra, (b) cut-off edges spectra and (c) Fermi edges spectra of $(NH_4)_xCs_{3-x}Cu_2I_5$ ($0 \leq x \leq 3$): x=0, x=0.6, x=0.9.

The valence band maxima (E_{VBM}) of $Cs_3Cu_2I_5$, $(NH_4)_{0.6}Cs_{2.1}Cu_2I_5$ and $(NH_4)_{0.9}Cs_{2.1}Cu_2I_5$ were determined and obtained from the following equation:

$$E_{VBM} = hv - E_{Cutoff} + E_{Fermi} \quad (1)$$

$$E_{CBM} = E_{VBM} + E_g \quad (2)$$

hv is the UV radiation energy of 21.2 eV, E_{Cutoff} is the binding energy of the second cutoff edge, E_{Fermi} is the difference between VBM and Fermi energy levels, E_{CBM} is the conduction band minimum.

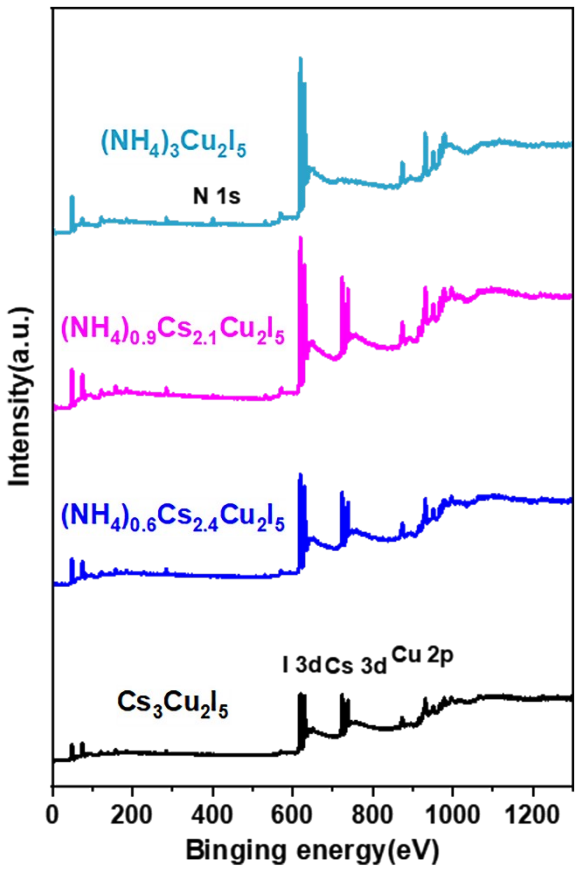

Fig. S9 The XPS survey spectra of $(NH_4)_xCs_{3-x}Cu_2I_5$ ($0 \leq x \leq 3$): x=0, x=0.6, x=0.9, x=3.

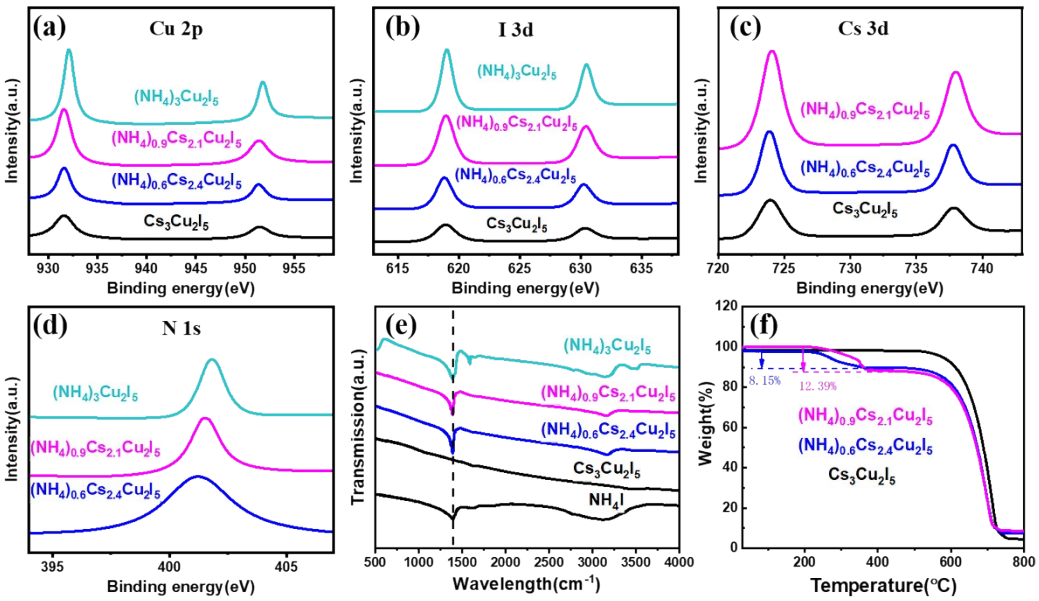

Fig. S10 HRXPS spectra of (a) Cu 2p; (b) I 3d; (c) Cs 3d; and (d) N 1s of $(NH_4)_xCs_{3-x}Cu_2I_5$: x=0, 0.6, 0.9, 3. (e) FTIR spectra of $(NH_4)_xCs_{3-x}Cu_2I_5$: x=0, 0.6, 0.9, 3 and pure NH_4I. (f) TGA spectra of $(NH_4)_xCs_{3-x}Cu_2I_5$: x=0, 0.6, 0.9.

Table S1 Diffraction angles corresponding to the main crystal planes of $(NH_4)_xCs_{3-x}Cu_2I_5$ ($0 \leq x \leq 3$): x=0, x=0.6, x=0.9.

	(122)	(312)	(222)	(131)	(004)
$Cs_3Cu_2I_5$	23.99°	25.55°	26.31°	28.05°	30.67°
$(NH_4)_{0.6}Cs_{2.4}Cu_2I_5$	24.25°	25.76°	26.56°	28.44°	30.84°
$(NH_4)_{0.9}Cs_{2.1}Cu_2I_5$	24.52°	25.99°	26.84°	28.75°	31.16°

Table S2 The lattice constants of $(NH_4)_xCs_{3-x}Cu_2I_5$ ($0 \leq x \leq 3$): x=0, x=0.6, x=0.9.

Material	a[a] [Å]	b[b] [Å]	c[c] [Å]	α[d] [°]	β[e] [°]	γ[f] [°]	V[g] [Å^3]
$Cs_2Cu_2I_5$	14.76	10.51	11.87	90	90	90	1842.13
$(NH_4)_{0.6}Cs_{2.4}Cu_2I_5$	14.78	10.49	11.69	89.39	88.35	89.75	1811.92
$(NH_4)_{0.9}Cs_{2.1}Cu_2I_5$	14.75	10.52	11.65	89.55	87.77	89.39	1805.42

Table S3 Tabulated fitted lifetime components of $(NH_4)_xCs_{3-x}Cu_2I_5$ ($0 \leq x \leq 3$): x=0, x=0.6, x=0.9.

	α_1 (%)	τ_1 (ns)	α_2 (%)	τ_2 (ns)	τ_{ave} (ns)
$Cs_3Cu_2I_5$	30.81	1456.60	69.19	9061.83	6718.66
$(NH_4)_{0.6}Cs_{2.4}Cu_2I_5$	31.62	2159.81	68.38	9781.90	7371.80
$(NH_4)_{0.9}Cs_{2.1}Cu_2I_5$	25.08	1605.69	74.92	8820.55	7011.06

The TRPL decay time, amplitude curves and τ_{ave}(average lifetime) are determined and obtained from the following equation, where equation (3) is a double-exponential equation:

$$y = y_0 + \alpha_1 e^{-x/\tau_1} + a_2 e^{-x/\tau_2} \quad (3)$$

$$\tau_{ave} = \frac{a_1\tau_1^2 + a_2\tau_2^2}{a_1\tau_1 + a_1\tau_2} \quad (4)$$

The pure $Cs_3Cu_2I_5$ shows a τ_2 of 9061 ns with α_2 of 69.2%. When the proportion of doped NH_4^+ (x) is 0.6, $(NH_4)_{0.6}Cs_{2.4}Cu_2I_5$ has the highest τ_2 (9782 ns) with the slightly decreased α_2 (68.4%), producing a longer average carrier lifetime (τ_{ave}) of 7372 ns than that of $Cs_3Cu_2I_5$ (6719 ns). Further increasing x to 0.9, lower τ_2 (8821 ns) but the largest α_2 (74.9%) resulted in a moderate τ_{ave} of 7011 ns. On the other hand, the undoped $Cs_3Cu_2I_5$ shows the smallest τ_1 (1456 ns) compared to those of $(NH_4)_{0.6}Cs_{2.4}Cu_2I_5$ (2160 ns) and $(NH_4)_{0.9}Cs_{2.1}Cu_2I_5$ (1606 ns).

1

Table S4. Optical parameter comparison of NH_4^+ doped Pb-based perovskites.

Ref	Formula	Morphology	Method	Emission peak	PLQY	Lifetime
6	$CsPb(I_{0.5}Br_{0.5})_3$	Nanocrystals	Ligand assisted re-precipitation	520nm	-	-
	$(NH_4)_{0.5}Cs_{0.5}Pb(I_{0.5}Br_{0.5})_3$	Nanocrystals	Ligand assisted re-precipitation	562nm	8%	-
7	$MAPbBr_3$	Quantum dots	Ligand assisted re-precipitation	456nm	-	17.60ns
	$MA_{0.5}(NH_4)_{0.5}PbBr_3$	Quantum dots	Ligand assisted re-precipitation	448nm	99.79%	19.94ns
8	$CsPbCl_2Br$	Powders	Ball milling	434nm	9.91%	12.20ns
	$Cs_{0.7}(NH_4)_{0.3}PbCl_2Br$	Powders	Ball milling	447nm	39.26%	15.06ns
9	$CsPbBr_3$	Quantum dots	Ligand assisted re-precipitation	509nm	35.8%	8.43ns
	$(NH_4)_xCs_{1-x}PbBr_3$	Quantum dots	Ligand assisted re-precipitation	509nm	85.3%	15.72ns
10	$CsPbI_3$	Films	Spin-coating	730nm	-	2.1ns
	$CsPbI_3$:NH_4^+	Films	Spin-coating	730nm	-	15.69ns

Table S5. Optical parameter comparison of $Cs_3Cu_2I_5$ perovskites regulated by various metal doping methods.

Ref	Formula	Morphology	Emission peak	PLQY	Lifetime
11	$Cs_3Cu_2I_5$	Powders	440nm	-	1.13us
	$Cs_3Cu_2I_5$:Na	Powders	440nm	-	1.45us
12	$Cs_3Cu_2I_5$	Films	440nm	76.2%	1088ns
	$Cs_3Cu_2I_5$:Tl	Films	520nm	64%	688ns
13	$Cs_3Cu_2I_5$	Powders	450nm	-	-
	$Cs_3Cu_2I_5$:Mn	Powders	562nm	-	39.84~51.64us
14	$Cs_3Cu_2I_5$	Microcrystals	445nm	-	1.23us
	$Cs_3Cu_2I_5$:Cd	Microcrystals	445,560nm	14.53%	0.86us
This work	$Cs_3Cu_2I_5$	Powders	450nm	20.90%	6719ns
	$(NH_4)_{0.6}Cs_{2.4}Cu_2I_5$	Powders	450nm	33.10%	7372ns

Results and Discussions of XPS, FTIR, TGA and the formation energy

To investigate the difference in the chemistry state of the elements between doped and undoped $Cs_3Cu_2I_5$ powders, their X-ray photoelectron spectra (XPS) are provided. The XPS survey spectra confirmed the presence of Cu, I, Cs and N in the samples (Fig. S9). In addition, the high-resolution spectra of each element (Cs 3d, Cu 2p, I 3d and N 1s) are shown in Fig. S10a-d. The Cu 2p spectra of $Cs_3Cu_2I_5$ and $(NH_4)_xCs_{3-x}Cu_2I_5$ consist of two distinct peaks at about 931.4 eV (Cu 2p3/2) and 951.3 eV (Cu 2p1/2), demonstrating the presence of monovalent Cu^+ in both materials[1,2]. With increasing ammonium content, the peak positions of I 3d signals shifted slightly towards lower binding energies (-0.05~0.1 eV). It is noteworthy that the N 1S and the Cs 3d peaks exhibit more pronounced shifts of about 0.1 eV towards higher binding energy with the substitution of Cs^+ by ammonium. These results suggest the change of the chemical environment of Cs and I ions after the NH_4^+ doping[3,4].

Fourier transform infrared spectroscopy (FTIR) measurements were conducted to investigate the interaction between NH_4^+ and Cu-I framework for further confirmation. As shown in Fig. S10e, both $(NH_4)_{0.6}Cs_{2.4}Cu_2I_5$ and $(NH_4)_{0.9}Cs_{2.1}Cu_2I_5$ samples have N–H asymmetric stretching vibration at 3000-3300 nm and N–H bending vibration at around 1390 nm, which shifts slightly to lower wavelengths as the proportion of ammonium ions increases. The bending of the N–H bond also appears in pure NH_4I, indicating that the H atoms are connected to the I atoms by hydrogen bonds in the crystal structure of $(NH_4)_xCs_{3-x}Cu_2I_5$[5]. According to the above XRD measurement, there was no NH_4I left in the $(NH_4)_{0.6}Cs_{2.4}Cu_2I_5$ and $(NH_4)_{0.9}Cs_{2.1}Cu_2I_5$ powders. Therefore, the FTIR and XPS results indicate that NH_4^+ has replaced Cs^+ in the lattice of perovskite and form NH–I bonding, which may favour the optical properties of perovskite[5].

The successful incorporation of NH_4^+ is likewise proven by the thermogravimetric analysis (TGA) data in Fig. S10f. The weight curves show that the $(NH_4)_{0.6}Cs_{2.4}Cu_2I_5$ and $(NH_4)_{0.9}Cs_{2.1}Cu_2I_5$ lost 8.15% and 12.39% of the original weights at 230~380 °C, respectively. These experimental values correspond very well with the calculated weight portion of NH_4I according to the formulae (7.97% and 12.34% for $(NH_4)_{0.6}Cs_{2.4}Cu_2I_5$ and $(NH_4)_{0.9}Cs_{2.1}Cu_2I_5$, respectively).

$$E_{form} = E^{total}_{(NH_4)_xCs_{3-x}Cu_2I_5} - E^{total}_{CsI} - E^{total}_{CuI} - E^{total}_{NH_4I} \quad (5)$$

The thermodynamic stability of (x=0, 0.6, 0.9, 2, 3) crystal structures has been studied using first-principles calculation, and the formation energy can be obtained using the equation (5). To limit the atomic

number of unit cells in the calculation, we chose the two approximate chemical formulas $(NH_4)_{0.5}Cs_{2.5}Cu_2I_5$ and $(NH_4)_1Cs_2Cu_2I_5$ to represent $(NH_4)_{0.6}Cs_{2.4}Cu_2I_5$ and $(NH_4)_{0.9}Cs_{2.1}Cu_2I_5$ respectively, because their stoichiometric ratios are close.

Reference

1 P. Yang, G. Liu, B. Liu, X. Liu,Y. Lou, J. Chen and Y. Zhao, *Chem. Commun.*, 2018, **54**, 11638-11641.
2 Li T, Mo X, Peng C, Q. Lu, C. Qi, X. Tao, Y. Ouyang and Y. Zhou, *Chem. Commun.*, 2019, **55**, 4554-4557.
3 T. Jun, K. Sim, S. Iimura, M. Sasase, H. Kamioka, J. Kim and H. Hosono, *Adv. Mater.*, 2018, **30**, 1804547.
4 Fang S, Wang Y, Li H, F. Fang, K. Jiang, Z. Liu, H. Li and Y. Shi, *J. Mater. Chem C.*, 2020, **8**, 4895-4901.
5 S. Tan, J. Shi, B. Yu, W. Zhao, Y. Li, Y. Li, H. Wu, Y. Luo, D. Li and Q. Meng, Adv. *Func. Mater.*, 2021, **31**, 2010813.
6 C. Wang, Y. Liu, X. Feng, C. Zhou, Y. Liu, X. Yu and G. Zhao, *Angew. Chem. Int. Ed.*, 2019, **58**, 11642-11646.
7 J. Deng, J. Xun, Y. Qin, M. Li and R. He, Chem. Commun., 2020, **56**, 11863-11866.
8 H. Xiao, H. Xiong, P. Li, L. Jiang, A. Yang, L. Lin, Z. Kang, Q. Yan and Y. Qiu, Chem. Commun., 2022, **58**, 3827-3830.
9 G. Getachew, W.-W. Huang T.-H. Chou, A. S. Rasal and J.-Y. Chang, *J. Colloid Interface Sci.*, 2020, **605**, 500-512.
10 S. Tan, J. Shi, B. Yu, W. Zhao, Y. Li, Y. Li, H. Wu, Y. Luo, D. Li and Q. Meng, Adv. Func. Mater., 2021, **31**, 2010813.
11 L. Xie, B. Chen and F. Zhang, et al., J. Lumin., 2021, **239**, 118333.
12 Q. Wang, M. Nikl, S. Cheng, G. Ren and Y. Wu, *Phys. Status Solidi RRL.*, 2021, **15**, 2100422.
13 P. Du, L. Luo and W. Cheng, *J Am Ceram Soc.*, 2020, **103**, 1149-1155.
14 J. Qu, S. Xu, Y. Cui and C. Wang, *Chem. Eur. J.*, 2022, **28**, e202200877.